Ordering of lowest conduction-band states in $(GaAs)_n/(AlAs)_m$ [111] superlattices

Z. Ikonić,* G. P. Srivastava, and J. C. Inkson
Physics Department, University of Exeter, Stocker Road, Exeter EX4 4QL, United Kingdom
(Received 12 May 1992)

The local empirical pseudopotential theory, implemented via the *S*-matrix layer method, was used to study the lowest conduction-band-states ordering in $(GaAs)_n/(AlAs)_m$ ($m=n, n\pm1, n\pm2$) superlattices grown in the [111] direction. The $(GaAs_n)/(AlAs)_n$ superlattice is found to have a direct band gap for all n, with far less prominent oscillations of conduction-band-states energies with n than is the case for [100] or [110] growth. Superlattices with $m>n$, however, are found to have indirect band gaps for small periods.

I. INTRODUCTION

Recently, there have been a number of both theoretical and experimental investigations on the conduction-band-states ordering in GaAs/AlAs superlattices (SL's), mostly for the [001] growth direction, and considerably less for the [110] and [111] ones. On the theoretical side, methods of various degrees of sophistication have been used: the effective-mass Kronig-Penney model, tight-binding, empirical pseudopotential, self-consistent pseudopotential models, and others.[1–8] For the [001] growth, theoretical results show reasonably good agreement with experiments. The case of [110] growth seems to have been explored only theoretically.[4–8] A common feature of both the [001]- and [110]-grown $(GaAs)_n/AlAs)_n$ SL's is that they are prominently indirect-band-gap materials for low-n values, and become direct (i.e., the absolute minimum of the conduction band comes to the folded Γ point) only for large enough n, typically $n\geq 8$ in the [001], and $n\geq 12$ in the [110] case.[7]

With advanced technology, it is now possible to grow high-quality superlattices in the [111] direction. Such SL's are of increasing interest, since they offer higher radiative efficiency than the traditional [001]-oriented structures can provide.[9] *Ab initio* theoretical studies have been reported for only very small-period [111] SL's such as GaAs/AlAs,[10] GaAs/GaP,[11] and GaAs/InAs.[12] As the SL period grows large, however, it becomes computationally very demanding to use the *ab initio* method. Indeed, the calculations in Refs. 10 and 11 were performed for layer-thickness indexes $n=1$ and 2, and then the results were extrapolated to the $n\rightarrow+\infty$ limit. On this basis, the $(GaAs)_n/(AlAs)_n$ [111] SL has been stated[10] to be a direct-band-gap material (in both reciprocal and direct spaces) for all n.

In this work we have used the empirical pseudopotential-layer method[13] to study the ordering of lowest conduction-band states in $(GaAs)_n/(AlAs)_m$ SL's, grown in the [111] direction, with $m=n$, $n\pm1$, $n\pm2$, and up to $m+n=20$. The nature of the lowest conduction band and its energy variation with the SL period thickness index $n+m$ has been determined. The results are compared and contrasted with our previous results, using the same method, for [001] and [110] SL's.

II. METHOD

The system is considered as a periodic repetition of a SL unit cell along the growth direction. One SL unit cell contains n monolayers of GaAs and m monolayers of AlAs. (A monolayer contains one straight and one slanted bond, and its thickness is $a/\sqrt{3}$, where a is the cubic lattice constant of the bulk material.) For each constituent material, we calculate propagating as well as evanescent electron states following a complex band-structure method.[13] The SL wave function in each material is expressed as a linear combination of the corresponding bulk states. These wave functions are matched at the interface between the two materials and, after propagation along the full SL period, the Bloch theorem is applied.

The complex band-structure scheme we employ uses a real-space description perpendicular to layer planes (i.e., along the SL axis), and a reciprocal-space description in layer planes.[14,15] In the case of [111]-grown SL, the complex band structure is calculated in the [111] direction. For a chosen in-plane projection $\mathbf{k}_\parallel$ of electron wave vector $\mathbf{k}=(\mathbf{k}_\parallel,\mathbf{k}_\perp)$, the Schrödinger equation is integrated and the perpendicular component $k_\perp(E)$—viz., the complex band structure—evaluated. Using M values of in-plane projections of three-dimensional (3D) reciprocal-lattice vectors ($\mathbf{g}_\parallel$), $2M$ states (i.e., values of complex $\mathbf{k}_\perp$) are calculated. Various bulk Brillouin-zone (BZ) points $\mathbf{k}$ are accessed by choosing appropriate $\mathbf{k}_\parallel$ values (projections of $\mathbf{k}$ on the surface BZ). In the case of [111] growth, all six equivalent X points of the bulk BZ are projected onto six distinct but symmetrically arranged points on the surface BZ. On the other hand, out of eight equivalent L points of bulk BZ, two [those at $(\pi/a)(1,1,1)$ and $(\pi/a)(-1,-1,-1)$, that we may call L_Γ] are projected onto $\bar{\Gamma}$ and the other six (that we may call L_X) onto the same surface BZ points as $\bar{X}$ [see Fig. 1(a)]. Therefore, the appropriate $\mathbf{k}_\parallel$ will "scan" either the Γ and L or X and L valleys. As compared to the all-reciprocal-space complex band-structure calculation (e.g., Ref. 16), the layer method turns out to be computationally more efficient by at least a factor of 4. However, unless a large number of 2D plane waves ($\mathbf{g}_\parallel$) are used, the results of the complex band-structure calculation using the layer method tend to artificially remove the energy de-

generacy of equivalent points in the bulk BZ which are mapped into inequivalent points on the surface BZ. The present calculations have been done with 31 2D plane waves, which correspond to a set of 89 3D vectors, up to and including the (331) star. This choice maintains the energy degeneracy between the above two types of L valleys to within a few meV.

With the complex band structure of bulk constituents of the SL calculated, the wave function is propagated across the layers and matched at the interfaces, as mentioned above. Using M plane waves ($\mathbf{g}_\parallel$) for in-plane wave-function expansion (corresponding normally to all 3D reciprocal-lattice vectors up to a full star), the number of electron states to be used for matching the wave function and its derivative at interfaces is $2M$ (half of them being incoming and the other half outgoing states[13]), and the dimensions of relevant matrices appearing in the calculation are $2M \times 2M$. Since the number of layers within the SL period and their widths may, in principle, be large, the presence of fast-decaying or -growing evanescent states generally makes the wave-function propagation extremely unstable if the T-matrix formulation is used. However, this problem can be circumvented if the S-matrix method is employed, instead (see Ref. 13 for details). Considering an N-layer structure, the amplitudes $\mathbf{a}_N$ and $\mathbf{b}_0$ of outgoing states can be related to the amplitudes $\mathbf{a}_0$ and $\mathbf{b}_N$ of incoming states via the S matrix (conveniently written in terms of four $M \times M$ blocks)[13] as

$$\begin{bmatrix} \mathbf{a}_N \\ \mathbf{b}_0 \end{bmatrix} = \begin{bmatrix} \mathbf{S}_{11} & \mathbf{S}_{12} \\ \mathbf{S}_{21} & \mathbf{S}_{22} \end{bmatrix} \begin{bmatrix} \mathbf{a}_0 \\ \mathbf{b}_N \end{bmatrix} . \tag{1}$$

In this specific calculation, it is enough to propagate the wave function, i.e., find the S matrix, in one full SL period (which means, say, from the left-hand side of one layer to the left-hand side of the next identical layer, belonging to the next period). The SL state, either propagating or evanescent, is found by demanding the wave function to be self-reproduced (within an exponential factor) upon its propagation across a full SL period d, i.e.,

$$\begin{aligned} \mathbf{a}_N &= \mathbf{a}_0 \exp(k_{\mathrm{SL}} d) , \\ \mathbf{b}_N &= \mathbf{b}_0 \exp(k_{\mathrm{SL}} d) , \end{aligned} \tag{2}$$

where k_{SL} is the SL-state wave vector, being purely imaginary for propagating SL states, and otherwise for evanescent states. One way to find the possible values of k_{SL} is to substitute Eq. (2) into Eq. (1), and solve for $\exp(k_{\mathrm{SL}} d)$, and another is to recast the SL-period S matrix in T matrix and diagonalize it, with its eigenvalues obviously being $\exp(k_{\mathrm{SL}} d)$. The first route leads to a nonlinear eigenvalue problem, similar to the one encountered in the all-reciprocal-space complex band-structure evaluation,[16] and is thus readily solvable, but involves more matrix inversions than the second procedure. Thus, we used the other route—remaking the T matrix from the final S matrix, to get

$$\begin{bmatrix} \mathbf{a}_N \\ \mathbf{b}_N \end{bmatrix} = \begin{bmatrix} (\mathbf{S}_{11} - \mathbf{S}_{12}\mathbf{S}_{22}^{-1}\mathbf{S}_{21}) & \mathbf{S}_{12}\mathbf{S}_{22}^{-1} \\ -\mathbf{S}_{22}^{-1}\mathbf{S}_{21} & \mathbf{S}_{22}^{-1} \end{bmatrix} \times \begin{bmatrix} \mathbf{a}_0 \\ \mathbf{b}_0 \end{bmatrix} = \mathbf{T} \begin{bmatrix} \mathbf{a}_0 \\ \mathbf{b}_0 \end{bmatrix} = \exp(k_{\mathrm{SL}} d) \begin{bmatrix} \mathbf{a}_0 \\ \mathbf{b}_0 \end{bmatrix} . \tag{3}$$

It turns out, however, that it is numerically extremely difficult, if not impossible, to invert blocks of the S matrix when a substantial number of states is included and layers are reasonably wide, because they are (numerically) almost singular. To be able to find SL states, we had to apply a truncation of the S-matrix blocks in such a way that highly evanescent states are discarded. We first sorted the arrays $\{\mathbf{a}_i\}$ and $\{\mathbf{b}_i\}$ so that they corresponded to increasingly evanescent states down the lists. The upper left-hand subblocks (say, $m_1 \times m_1$ each, with $m_1 < \mathbf{M}$) of the S-matrix blocks, corresponding to propagating or less evanescent states only, were extracted, and then rejoined to make the truncated S matrix. Equation (3) is then applied to this truncated S matrix. Stable results were obtained for m_1 in the range 4–7, with essentially no difference in SL-state energies. For larger m_1, especially when large-period SL's are considered, the scheme becomes unstable due to the presence of grossly evanescent states. Analysis of the results obtained with $m_1 = 4$–7 shows, however, that these evanescent states make insignificant overall contribution to SL states. We should point out here that this procedure is not at all equivalent

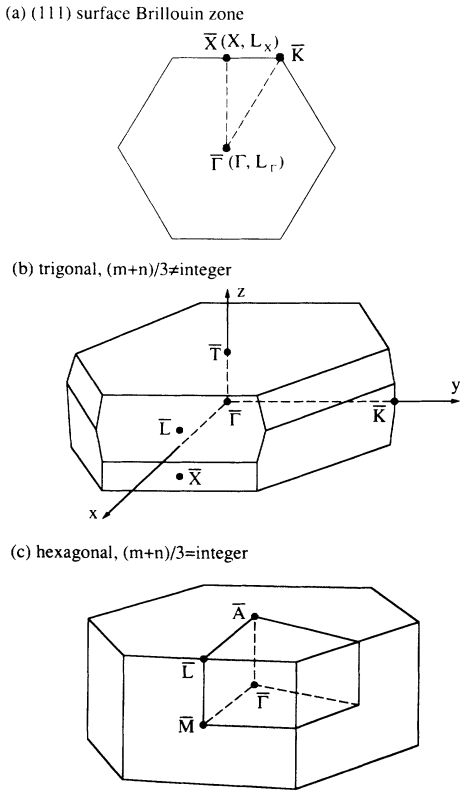

FIG. 1. (a) The (111) surface Brillouin zone with mapping of some bulk-BZ points and the superlattice zone of the [111]-grown $(GaAs)_n/(AlAs)_m$ SL, being (b) simple trigonal in case the SL period $n+m$ is not a multiple of 3, and (c) simple hexagonal if $n+m$ is a multiple of 3 (Ref. 11). The SL growth direction is along z. Folding of various bulk-BZ points into points of the SL BZ is given in Table I.

TABLE I. Folding of some important bulk-BZ points into superlattice BZ points (Fig. 1) for various possible values of the superlattice period $n+m$.

	X	L_X	Γ	L_Γ
$(n+m)/2$=integer $(n+m)/3$=integer	$\bar{M}$	$\bar{M}$	$\bar{\Gamma}$	$\bar{\Gamma}$
$(n+m)/2\neq$integer $(n+m)/3$=integer	$\bar{M}$	$\bar{L}$	$\bar{\Gamma}$	$\bar{A}$
$(n+m)/2$=integer $(n+m)/3\neq$integer	$\bar{X}$	$\bar{X}$	$\bar{\Gamma}$	$\bar{\Gamma}$
$(n+m)/2\neq$integer $(n+m)/3\neq$integer	$\bar{X}$	$\bar{L}$	$\bar{\Gamma}$	$\bar{T}$

to using the same number (m_1) of states in a T-matrix formulation of the SL problem, because a small number of $k_\perp$ states would imply that an equally small number of $\mathbf{g}_\parallel$ components of the wave function and its derivative are really matched at the interfaces, which may not even (and typically cannot) include all the components of the in-plane projection of a full star of reciprocal-lattice vectors. In the S-matrix formulation, however, the matching of even very high $\mathbf{g}_\parallel$ components of the wave function is properly done, and only when it comes to the final S matrix (relating $k_\perp$ states, not $\mathbf{g}_\parallel$ components) it is truncated, and highly evanescent states are neglected, i.e., they had to be included only temporarily, to obtain matching of higher $\mathbf{g}_\parallel$ components.

For a chosen $\mathbf{k}_\parallel$, SL states are determined from the calculated k_{SL} values. They are interpreted in terms of constituent bulk semiconductor states, folded along the SL axis. In that sense, this calculation is not of the supercell type,[5,10–12] but the calculated states can be uniquely related to the corresponding states in the SL BZ [Figs. 1(b) and 1(c)]. In our discussion, the points of the SL BZ, obtained by folding bulk-BZ points, are denoted by a bar above the corresponding bulk-BZ state. As for the important points Γ, X, and L of the bulk BZ, we find that in the case where the SL period includes an even number of monolayers, i.e., $n+m$ =even (cases actually explored in Refs. 10–12, since $n=m$ therein), points Γ and L_Γ fold to the same point of SL BZ, which we shall denote $\bar{\Gamma}(=\bar{L}_\Gamma)$. Similarly, points X and L_X of the bulk BZ both fold into the same point $\bar{X}(=\bar{L}_X)$ of SL BZ (also denoted $\bar{F}$ in Ref. 12). However, if $n+m$ =odd, L_Γ folds into $\bar{L}_\Gamma$, not coinciding with $\bar{\Gamma}$ and, similarly, the folded L_X ($\bar{L}_X$) does not now coincide with $\bar{X}$. The shape of the SL BZ depends on whether or not $n+m$ is a multiple of 3, and not of 2, as shown in Figs. 1(b) and 1(c). In Table I we map some important bulk-BZ points in the SL BZ for various values of the SL period $n+m$.

III. RESULTS AND DISCUSSION

In the numerical calculations, we used the Caruthers-Lin Chung set of the pseudopotential form factors[17] for GaAs and AlAs, since they give a reasonably good description of various band gaps in both the materials. Calculated with 31 2D plane waves, the energies at a few symmetry points measured from the conduction-band minimum at the Γ point are $E_X=0.486$ eV, $E_L=0.304$ eV, and a band gap of 1.514 eV at Γ for GaAs, and $E_X=-0.578$ eV, $E_L=-0.327$ eV, and a band gap of 2.812 eV at Γ for AlAs. Because of neglect of charge transfer in this model, band discontinuities for different valleys at the GaAs/AlAs interface do not quite agree with experiment. The amount of this disagreement is different for Γ, X, and L points, which reflects differences in the theoretical and experimental bulk-band structures. This may be partly corrected by introducing an appropriate shift of the bulk-band structure of one of the semiconductors. In this work, we employed a downward shift of the AlAs band structure by $V_{\mathrm{off}}=0.05$ eV, which gives reasonable agreement of discontinuities at the interface with those obtained by applying the frequently used $\Delta E_c/\Delta E_v=65/35$ rule to the experimental valley energies[18] (Table II). In view of a significant spread in experimental values for both the bulk band gaps and the $\Delta E_c/\Delta E_v$ ratio, the overall comparison between the two sets of values in Table II should be acceptable. Also listed in Table II are the various band discontinuities used in the theoretical work of Wei and Zunger.[19] These workers used experimental data for conduction-band energies and their theoretical data for ΔE_v to obtain these discontinuity values. Clearly, the value of $\Delta E_c(L)$ used in their work is higher than our value or the experimentally extracted value by more than 0.6 eV.

The calculations for SL valence-band states were performed by taking spin-orbit coupling into account. Values of spin-orbit coupling constants in GaAs and AlAs are chosen so that the splitoff valence band is below the heavy- and light-hole valence bands in these two materials by 0.34 and 0.30 eV, respectively.

In all the $(\mathrm{GaAs})_n/(\mathrm{AlAs})_m$, $m=n$, $n\pm1$, $n\pm2$ SL's investigated in this work, the lowest SL state accessed by $\mathbf{k}_\parallel=0$ always occurs at the SL $\bar{\Gamma}$ point, never at $\bar{L}_\Gamma$ if it is distinct from $\bar{\Gamma}$. If the $\bar{X}$ and $\bar{L}_X$ points are distinct, the lowest state is almost always at $\bar{X}$, with just a single exception, as discussed below.

The results for the $(\mathrm{GaAs})_n/(\mathrm{AlAs})_n$ SL, with equal layer widths, are given in Fig. 2. Energies of the lowest conduction-band states (taken as the bottoms of minibands) are given on the $+E$ axis, measured from the GaAs conduction-band edge at the Γ point, and those of valence-band states on the $-E$ axis, measured from the GaAs valence-band top (i.e., no band gap is displayed). Full lines correspond to conduction-band states at the $\bar{\Gamma}$

TABLE II. Band discontinuities (in eV) at the GaAs/AlAs interface obtained by downshifting AlAs bands by $V_{\mathrm{off}}=0.05$ eV, compared with the corresponding values calculated from the 65/35 rule applied to valley energies in Ref. 18. Also listed are the values used in the theoretical work of Wei and Zunger (Ref. 19).

	This work	"65/35" rule	Ref. 19
$\Delta E_c(\Gamma)$	0.778	1.036	1.16
$\Delta E_c(X)$	−0.286	−0.290	−0.20
$\Delta E_c(L)$	0.157	0.084	0.77
$\Delta E_v(\Gamma)$	0.520	0.558	0.45

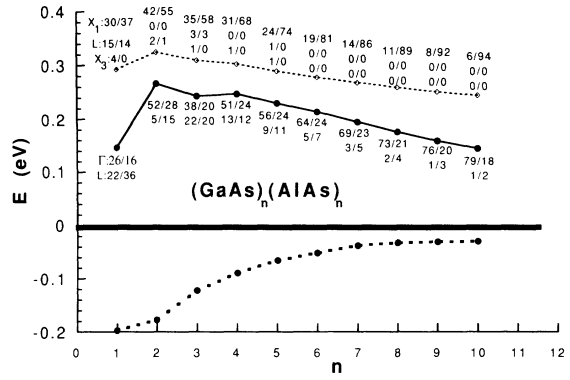

FIG. 2. Energies of the lowest conduction-band states at $\bar{\Gamma}$ (solid lines) and $\bar{X}$ or $\bar{L}_X$ (broken lines) points in the SL BZ, and of the highest valence-band states at $\bar{\Gamma}$ (dotted lines), in the [111]-grown $(GaAs)_n/(AlAs)_n$ SL's. Energies of the conduction-band states are measured from the GaAs conduction-band edge at Γ ($+E$ axis) and those of valence-band states from the GaAs valence-band top at Γ ($-E$ axis), both being represented by the thick horizontal line at $E=0$ (i.e., the GaAs band gap is not displayed). The composition of SL conduction-band states in GaAs and AlAs layers, in terms of relative contributions of Γ, X_1, X_3, and L bulk states (in percent), is given along the lines from which the degree of wave-function localization can be deduced (see text for more detailed explanation of the notation used). Thickness of one monolayer is $a/\sqrt{3}=0.326$ nm (a is the cubic-lattice constant).

($\bar{L}_\Gamma$) point of the SL BZ, and broken lines to those at the $\bar{X}$ ($\bar{L}_X$) points. Clearly, the $(GaAs)_n/(AlAs)_n$ SL is a direct band-gap material for all n. We find that both the $\bar{\Gamma}$ and $\bar{X}$ states are lower in energy for the $n=1$ than for the $n=2$ SL. As n increases beyond 2, the energy of the $\bar{X}$ state gradually decreases. However, the energy of the $\bar{\Gamma}$ state shows an oscillatory change up to $n=4$, and thereafter gradually decreases with increasing n. Compared with the [100] and [110] SL's,[7] the amplitudes of such oscillations are much smaller for the [111] SL's. In Fig. 2 we also give the "composition" of SL-state wave functions Ψ_{SL}, normalized to unity in the SL period. The notation we use is the following—e.g., $\Gamma{:}c_1/c_2$, $L{:}c_3/c_4$ means that c_1 percent of the total $|\Psi_{SL}|^2$ is the Γ state accumulated in the GaAs layer and c_2 in the AlAs layer, while c_3 percent of total $|\Psi_{SL}|^2$ is the L state in GaAs and c_4 in AlAs (all percentages are rounded off to the nearest whole number, and all add up to 100%). Thus, summation of the percentages in Fig. 2 by columns gives the degree of wave-function localization, and summation by rows the relative contribution of relevant bulk states to the SL state. By inspecting the data in Fig. 2 we see that neither the $\bar{\Gamma}$ nor the $\bar{X}$ SL state in the $(GaAs)_1/(AlAs)_1$ SL is significantly localized in any of the two layers, and that heavy mixing of the corresponding bulk states takes place. As for the $\bar{\Gamma}$ state in larger-period SL's, the absence of strong localization and remarkable mixing of Γ and L bulk states is significant for $N\leq 5$, beyond which the SL acquires an effective-mass-like behavior—a single state (in this instance Γ) dominates in both layers, and is distributed in accordance with the well and/or barrier picture. Somewhat surprisingly, the SL states at $\bar{X}$ are found to behave like this much earlier, as early as $n=2$. These states are almost purely X_1 in character, the admixture of L and X_3, if any, being only marginal.

Our results for $(GaAs)_n/(AlAs)_n$ should be taken as complementary to the *ab initio* work of Wei and Zunger[10] on ultrathin (111) SL's. For $n=1$ and 2 (the only n values considered by Wei and Zunger) our results are in qualitative agreement with their work. Quantitatively, however, there are disagreements. For $n=1$ we have calculated the lowest conduction band to be at $E_c+0.14$ eV, whereas after band-gap correction Wei and Zunger have calculated this state at $E_c+0.45$ eV. For $n=2$ our result for the lowest conduction band is $E_c+0.27$ eV, whereas the result of Wei and Zunger is $E_c+0.56$ eV. Disagreements of magnitudes similar to those between our results[7] and those of Wei and Zunger[19] have also been noted for [100]-grown SL's. Such disagreements are a consequence of many factors. The present work uses empirically fitted pseudopotential form factors at the experimental lattice constant, implements an *ad hoc* $V_{\rm off}$ to obtain reasonable values of discontinuities at Γ, X, and L, and does not account for any charge redistribution in the manner achieved in a self-consistent procedure. On the other hand, the results of Wei and Zunger are based on a fully self-consistent procedure, using a theoretically determined lattice constant, a tetragonal distortion along the growth direction, and a rather *ad hoc* procedure for correcting the band-gap underestimation that arises within the local-density approximation. It was noted earlier in this section (and Table II) that the Wei-Zunger estimate[19] of $\Delta E_C(L)$ is far too big compared to our choice or the value extracted from the 65/35 rule applied to experimental values of valley energies. It is useful at this point to assess the role of self-consistency in such calculations. For this, we compare two of our previous calculations[5,7] on the (100) SL with $n=1$. The energy of the lowest conduction band is at $E_c+0.14$ eV from the empirical pseudopotential-layer method,[7] and at $E_c+0.16$ eV from the self-consistent local pseudopotential method within the X_α scheme.[5] Thus, the role of self-consistency alone is not sufficient to explain the disagreement between our results and those of Wei and Zunger. Also, the earlier work of Wei and Zunger[19] on the (100) SL's shows that the energy location of the lowest conduction band for $n=1$ does not change appreciably when the structure is relaxed fully. From the above two observations it would appear that the correction of band gaps, specially of the L valley, in the work of Wei and Zunger makes a significant contribution to the disagreement between our results and theirs for ultrathin SL's (viz., $n=1$ and 2) with a large L contribution.

The lowest conduction-band states for $(GaAs)_n/(AlAs)_m$ SL's with the GaAs layer width exceeding that of AlAs are given in Fig. 3 ($m=n-1$), and Fig. 4 ($m=n-2$). These SL's are even more prominently direct-band-gap materials, which could have been expected from the effective-mass model, with the bulk-Γ states more dominant and more confined to GaAs than in $n=m$ SL's. Now there are no oscillators in state energies

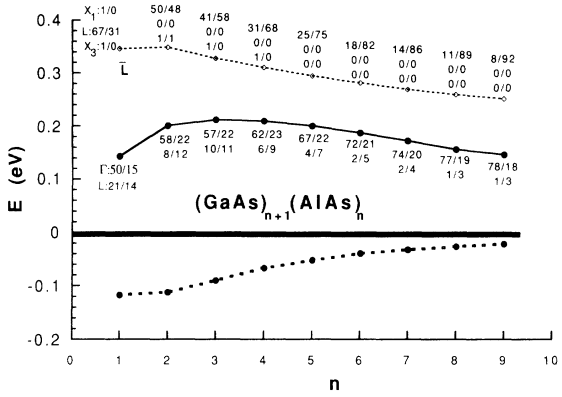

FIG. 3. Same as in Fig. 2, but for $(GaAs)_{n+1}/(AlAs)_n$ SL's. Note that the lowest indirect state is at the $\bar{L}$ point of the SL BZ [Fig. 1(c)], unlike all the other cases in Figs. 2–6, where it is at $\bar{X}$ or $\bar{M}$, depending on the value of $n+m$.

as n increases. It is interesting that the lowest indirect state in the $(GaAs)_2/(AlAs)_1$ SL is predominantly L-like in character, and is positioned at the $\bar{L}_X$, not the $\bar{X}$ point (these two differ when $m+n$ is odd), the lowest $\bar{X}$ state being some 30 meV above (not depicted in Fig. 3). For ($n=3$, $m=2$) and beyond, however, $\bar{X}$ states are lower than $\bar{L}_X$ state and have an X-like character. This feature is even more pronounced in $(GaAs)_{n+2}/(AlAs)_n$ SL's, where purely X-like states occur at $n=4$ and beyond. For the (3,1) and (4,2) SL's the lowest indirect states are dominantly L-like, and for the (5,3) SL more X-like, but with a high admixture of L states. However, since $m+n$ is now even, $\bar{X}$ and $\bar{L}_X$ points coincide, and all these indirect SL states take the same position in the SL BZ. It is also worth noting that $\bar{X}$ and $\bar{L}_X$ SL-state energies for $n \leq 4$ in both cases are above both the L point in GaAs and the X point in AlAs, so there are different propagating states in both the SL layers, but this alone is not enough for the X-L mixing to be significant—mixing is favored by coincidence of $\bar{X}$ and $\bar{L}_X$ SL BZ points, which takes place in $(GaAs)_{n+2}/(AlAs)_n$ SL's only.

If the AlAs layer width exceeds that of GaAs by at least one monolayer, the [111]-grown SL becomes an indirect band-gap material for low-enough n ($n<3$), as given in Fig. 5. Such a behavior is also qualitatively in

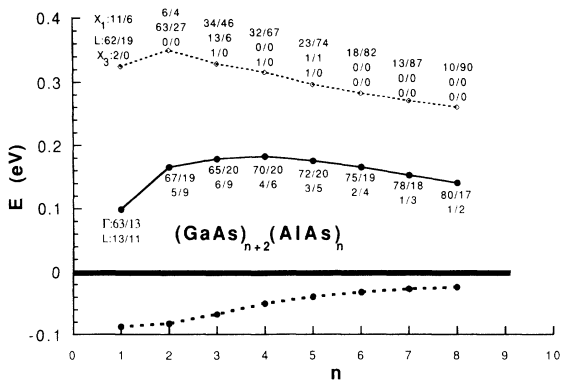

FIG. 4. Same as in Fig. 2, but for $(GaAs)_{n+2}/(AlAs)_n$ SL's.

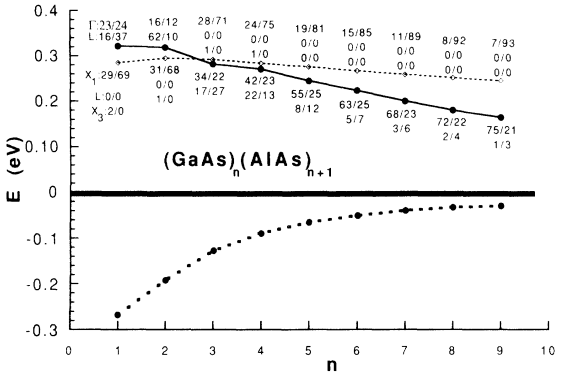

FIG. 5. Same as in Fig. 2, but for $(GaAs)_n/(AlAs)_{n+1}$ SL's.

accordance with the effective-mass picture, where the barriers for Γ electrons and wells for X electrons grow larger, inducing the SL $\bar{\Gamma}$ levels to be pushed up and the $\bar{X}$ levels to sink and go below the $\bar{\Gamma}$ levels. Certainly this affects only thin-layer SL's (including the ones that became indirect, Fig. 5), and not those with very thick layers, where the lowest miniband energies will eventually coincide with the corresponding conduction-band edges (Γ of GaAs for $\bar{\Gamma}$ states, X of AlAs for $\bar{X}$ states). For even wider AlAs layers ($m=n+2$), the $(GaAs)_n/(AlAs)_{n+2}$ SL remains indirect up to $n<5$ (Fig. 6). As given in Figs. 5 and 6, in neither of these two cases do bulk-L states play a significant role in indirect SL states, and the wave-function localization to AlAs is clearly visible even for very small periods. As for the SL valence-band states, in all the above cases, they show similar behavior, i.e., their energies tend towards the bulk-GaAs valence-band top as the SL period increases. These states are all heavy-hole states positioned at the $\bar{\Gamma}$ point of the SL BZ, with no significant admixture of light-hole or splitoff band states. For not very low periods ($n \geq 5$), due to the large heavy-hole mass and barrier height (cf. Table II), these energies depend on GaAs layer width only, and the states (hole minibands) are extremely narrow, but in cases where the GaAs layers are only one or two monolayers thick, the influence of the barrier (AlAs) width is considerable. For example, as

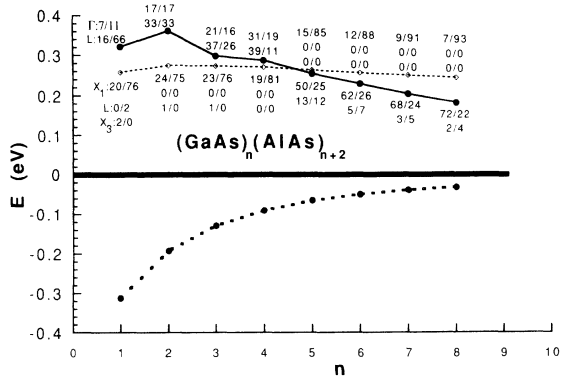

FIG. 6. Same as in Fig. 2, but for $(GaAs)_n/(AlAs)_{n+2}$ SL's.

seen in Figs. 2–6, when n changes from 1 to 2 there is very little rise in the heavy-hole state for the SL's $(GaAs)_m/(AlAs)_n$ with $m=n$, $n+1$, and $n+2$, but there is a uniform rise in this energy with increasing n for $(GaAs)_n/(AlAs)_m$ with $m=n+1$ and $n+2$.

IV. CONCLUSION

Using the empirical pseudopotential method in the S-matrix implementation, we have investigated the ordering of the lowest conduction-band states in the [111]-growth $(GaAs)_n/(AlAs)_m$ ($m=n$, $n\pm1$, $n\pm2$) SL's. The $(GaAs)_n/(AlAs)_n$ SL is found to be a direct-band-gap material for all n, in accordance with the conclusions of Ref. 10, as are all $(GaAs)_n/(AlAs)_m$ ($m<n$) SL's. For $m>n$, however, these SL's are indirect for lower n values ($n<3$ in the $m=n+1$ case, and $n<5$ in the $m=n+2$ case), implying that these SL's are quite sensitive to one- or two-monolayer variations in their structure. For large-enough GaAs layer widths (typically $n\geq6$) the $\bar{\Gamma}$ SL states become predominantly ($\geq90\%$) composed of bulk-Γ states (although the admixture of bulk-L states remains up to much larger n), and their energies are essentially determined by the GaAs layer width and, in this sense, $\bar{\Gamma}$ states acquire effective-mass type of behavior. As for the $\bar{X}$ SL state, mixing of the corresponding bulk states is found to be almost negligible, except for very low periods. These states are mostly composed of X_1 bulk states, with neither L nor X_3 making a noticeable contribution. In this sense the $\bar{X}$ SL states of the [111]-grown GaAs/AlAs SL seem to be almost ideal candidates for the effective-mass type of calculation (provided that the nonparabolicity along the principal ellipsoid axis of X valleys, known to be significant,[20] is taken into account).

ACKNOWLEDGMENTS

Z. I. acknowledges Exeter University, Exeter, U.K., and the SERC (U.K.) for financial support. The authors would like to thank the SERC, U.K., for the use of its computational facilities through the CSI scheme.

*On leave from the Faculty of Electrical Engineering, University of Belgrade, Bulevar Revolucije 73, 11000 Belgrade, Serbia, Yugoslavia.

[1]S.-H. Wei and A. Zunger, J. Appl. Phys. **63**, 5794 (1988).
[2]S. B. Zhang, M. S. Hybertson, M. L. Cohen, S. G. Louie, and D. Tomanek, Phys. Rev. Lett. **63**, 1495 (1989).
[3]S. Gopalan, N. E. Christensen, and M. Cardona, Phys. Rev. B **39**, 5165 (1989).
[4]R. J. Gordon, Z. Ikonić, and G. P. Srivastava, Semicond. Sci. Technol. **5**, 269 (1990).
[5]G. P. Srivastava, R. J. Gordon, and Z. Ikonić, Superlatt. Microstruct. **9**, 43 (1991).
[6]B. Samra, R. J. Gordon, and G. P. Srivastava, Semicond. Sci. Technol. **4**, 322 (1989).
[7]Z. Ikonić, J. C. Inkson, and G. P. Srivastava, Semicond. Sci. Technol. **7**, 648 (1992).
[8]R. Eppenga and M. F. H. Schuurmans, Phys. Rev. B **38**, 3541 (1988).
[9]T. Hayakawa, K. Takahashi, M. Kondo, T. Suyama, S. Yamamoto, and T. Hijikata, Phys. Rev. Lett. **60**, 349 (1988).
[10]S.-H. Wei and A. Zunger, Appl. Phys. Lett. **53**, 2077 (1988).
[11]R. G. Dandrea and A. Zunger, Phys. Rev. B **43**, 8962 (1991).
[12]R. Magri and C. Calandra, Phys. Rev. B **40**, 3896 (1989).
[13]D. Y. K. Ko and J. C. Inkson, Phys. Rev. B **38**, 9945 (1988).
[14]M. G. Burt, J. Phys. C **13**, 1825 (1980).
[15]P. Dzwig, M. G. Burt, J. C. Inkson, and V. Crum, J. Phys. C **15**, 1187 (1982).
[16]S. Brand and D. T. Hughes, Semicond. Sci. Technol. **2**, 607 (1987).
[17]E. Caruthers and C.-L. Chung, Phys. Rev. B **17**, 2705 (1978).
[18]S. Adachi, J. Appl. Phys. **58**, R1 (1985).
[19]S.-H. Wei and A. Zunger, J. Appl. Phys. **63**, 5794 (1988).
[20]M. V. Fischetti, IEEE Trans. Electron Devices **ED-38**, 634 (1991).